ACS OMEGA

http://pubs.acs.org/journal/acsodf

Article

Nature of Linear Spectral Properties and Fast Relaxations in the Excited States and Two-Photon Absorption Efficiency of 3-Thiazolyl and 3-Phenyltiazolyl Coumarin Derivatives

Yevgeniy O. Shaydyuk, Nataliia V. Bashmakova, George V. Klishevich, Andriy M. Dmytruk, Olexiy D. Kachkovsky, Iaroslav B. Kuziv, Igor Ya. Dubey, Kevin D. Belfield,* and Mykhailo V. Bondar*

Cite This: *ACS Omega* 2023, 8, 11564−11573

Read Online

ACCESS | Metrics & More | Article Recommendations | Supporting Information

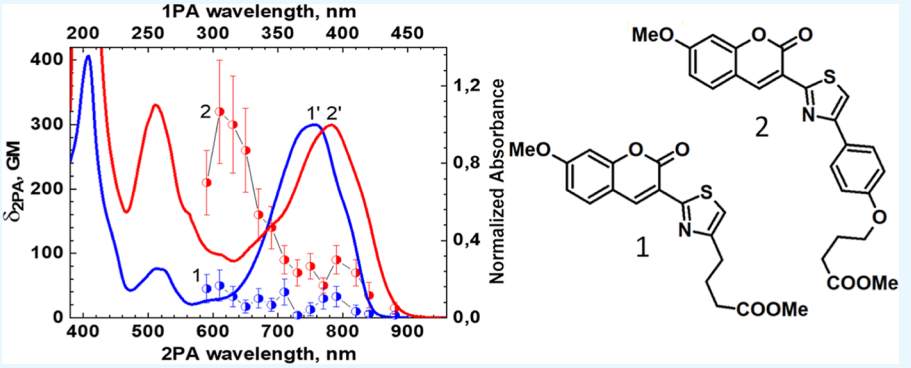

ABSTRACT: Coumarin-based fluorescent agents play an important role in the manifold fundamental scientific and technological areas and need to be carefully studied. In this research, linear photophysics, photochemistry, fast vibronic relaxations, and two-photon absorption (2PA) of the coumarin derivatives, methyl 4-[2-(7-methoxy-2-oxo-chromen-3-yl)thiazol-4-yl]butanoate (**1**) and methyl 4-[4-[2-(7-methoxy-2-oxo-chromen-3-yl)thiazol-4-yl]phenoxy]butanoate (**2**), were comprehensively analyzed using stationary and time-resolved spectroscopic techniques, along with quantum-chemical calculations. The steady-state one-photon absorption, fluorescence emission, and excitation anisotropy spectra, as well as 3D fluorescence maps of 3-hetarylcoumarins **1** and **2** were obtained at room temperature in solvents of different polarities. The nature of relatively large Stokes shifts (∼4000−6000 cm^{-1}), specific solvatochromic behavior, weak electronic $\pi \rightarrow \pi^*$ transitions, and adherence to Kasha's rule were revealed. The photochemical stability of **1** and **2** was explored quantitatively, and values of photodecomposition quantum yields, on the order of $\sim 10^{-4}$, were determined. A femtosecond transient absorption pump−probe technique was used for the investigation of fast vibronic relaxation and excited-state absorption processes in **1** and **2**, while the possibility of efficient optical gain was shown for **1** in acetonitrile. The degenerate 2PA spectra of **1** and **2** were measured by an open aperture z-scan method, and the maximum 2PA cross-sections of ∼300 GM were obtained. The electronic nature of the hetaryl coumarins was analyzed by quantum-chemical calculations using DFT/TD-DFT level of theory and was found to be in good agreement with experimental data.

1. INTRODUCTION

The development and investigation of different types of coumarin derivatives remain subjects of continuing interest for a number of important research areas, including organic electronics,[1,2] nonlinear optics, and lasing,[3−7] 3D microfabrication and optical data storage,[8−10] sensing technologies,[11−15] biomedical probes and reactants,[16−18] and one- and two-photon photodynamic therapy (PDT).[19,20] Coumarin derivatives exhibit a large variety of linear steady-state and time-resolved photophysical properties,[21−33] which depend on the specific substituents in different positions of the molecular architecture[18,24,25,27,34,35] and solute−solvent interactions.[2,21,22,26,36,37] These characteristics afford the ability to tune emission efficiency,[21,38] the values of Stokes shifts,[34] binding abilities,[23,39] and photochemical stability[40] along with harnessing the fast relaxation processes in the ground and excited electronic states of coumarins for a number of applications.[28−33] It should be mentioned that notable efforts were made for improving and making practical use of the two-photon absorption (2PA) properties of coumarin derivatives in

Received: February 1, 2023
Accepted: March 7, 2023
Published: March 16, 2023

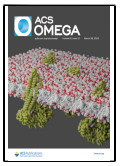

the microfabrication,[41] biomedicine,[42] fluorescence microscopy,[43] and PDT[19] research fields.

In this research, we studied two particular hetaryl coumarin derivatives with extended chromophore systems and expected potential for some important technological areas, including two-photon fluorescence microscopy, bioimaging, and optical data storage. The nature of linear steady-state and time-resolved photophysical and photochemical properties of 3-hetarylcoumarins containing thiazolyl and phenylthiazolyl fragments, methyl 4-[2-(7-methoxy-2-oxo-chromen-3-yl)-thiazol-4-yl]butanoate (**1**) and methyl 4-[4-[2-(7-methoxy-2-oxo-chromen-3-yl)thiazol-4-yl]phenoxy]butanoate (**2**), were investigated, along with the fast relaxation processes in the excited electronic states and 2PA efficiency under femtosecond excitation. The main electronic parameters of **1** and **2** were also analyzed using density functional theory (DFT)/time-dependent (TD)-DFT quantum-chemical calculations, yielding quite reasonable agreement with experimentally determined properties.

2. EXPERIMENTAL SECTION

2.1. Synthesis and Linear Photophysical and Photochemical Characterization of 3-Hetarylcoumarins 1 and 2. The synthesis of coumarin **1** (see the chemical structure in Figure 1) was based on Knoevenagel condensation between

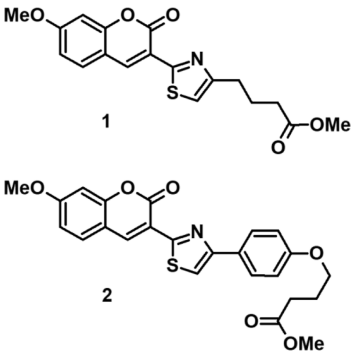

Figure 1. Chemical structures of the coumarin derivatives **1** and **2**.

the corresponding derivatives of salicylaldehyde and 2-cyanomethylthiazole and is comprehensively described in ref 44. In contrast to that previously reported,[45] coumarin derivative **2** was prepared by an optimized procedure (Scheme 1), where one-pot thiazole synthesis commenced from acetophenone **A**. It should be mentioned that there are a limited number of papers describing the one-pot Hantzsch thiazole synthesis in the case of 2,4-disubstituted thiazole derivatives. The general synthetic scheme can be described as a two-step procedure: generation of α-halogenoketones, followed by their reaction with thioamides. In this work, bromination of compound **A** with bromine in ethanol at ~45 °C was used at the first step. Then, the reaction mixture was degassed in vacuo to facilitate HBr elimination, while excess MgO was added for the neutralization of HBr.

In the second step, 2-cyanothioacetamide was added and refluxed ~1 h. Compound **C** was obtained in 54% yield after double chromatographic purification. Iminocoumarin **D** was obtained by condensation of **C** and 2,4-dihydroxybenzaldehyde in the presence of piperidine as a catalyst in methanol at reflux. Fast hydrolysis of the imino group of intermediate **D** was achieved in the DMF−HCl mixture, in contrast to the previously used HCl addition to the reaction mixture.[44] HCl was then neutralized with $NaHCO_3$, and aqueous NaOH and methanol were added. Compound **E** was purified by recrystallization from pyridine, and the resulting pyridinium salt was transformed into the free acid by precipitation in aq acetic acid. Compound **2** was obtained by the reaction of **E** with dimethyl sulfate in DMF in the presence of potassium carbonate. It was purified by recrystallization from pyridine, providing a purity of over 97% by LC−MS. The synthetic details are presented in the Supporting Information.

Linear steady-state and time-resolved photophysical characteristics, along with the photochemical parameters of the 3-hetarylcoumarins **1** and **2**, were obtained in air-saturated spectroscopic grade benzene (BNZ) and acetonitrile (ACN) at room temperature. These commercially purchased solvents were additionally purified via distillation. The steady-state absorption spectra were measured with the Shimadzu UV-2450 (Shimadzu Europe) spectrophotometer, using a standard 1 cm path length quartz cuvettes and solute concentrations, $C \sim (4-6) \times 10^{-5}$ M. The steady-state emission measurements, including corrected fluorescence, excitation, and excitation anisotropy spectra, were performed in 1 cm path length fluorometric quartz cuvettes with the CM 2203 (Solar, Belarus) spectrofluorimeter. All emission parameters of **1** and **2** were obtained for dilute solutions ($C \leq 10^{-6}$ M) to reduce possible reabsorption effects.[46]

The determination of the fluorescence quantum yields, Φ_{fl}, of **1** and **2** was performed by a relative method with 9,10-diphenylanthracene in cyclohexane as a standard.[46] The values of emission lifetimes, τ_{fl}, were determined from the corresponding decay curves for **1** and **2** using the Life Spec-II (Edinburgh Instr. Ltd.) spectrofluorimeter with a single photon-counting system and picosecond excitation. The steady-state fundamental anisotropy, $r_0(\lambda)$, was obtained from the experimentally determined excitation anisotropy spectrum, $r(\lambda) = r_0(\lambda)/(1 + \tau_{fl}/\theta)$ (θ is the rotational correlation time), which was measured in a high-viscosity solvent (glycerol at room temperature), where $\theta \gg \tau_{fl}$ and $r(\lambda) \approx r_0(\lambda)$.[47] It should be mentioned that $r_0 = (3\cos^2\alpha - 1)/5$ (α is the angle between corresponding absorption, μ_{01} ($S_0 \rightarrow S_1$), and emission, μ_{10} ($S_1 \rightarrow S_0$), transition dipoles; S_0 and S_1 are the ground and first excited electronic states, respectively).[46]

Photochemical properties of **1** and **2** were investigated in air-saturated solutions using CW laser irradiation in the main absorption band (excitation wavelength, λ = 400 nm; average laser power ≈ 70 mW). The efficiency of photodecomposition processes was estimated quantitatively by measuring the photodecomposition quantum yields, Φ_{ph}, which can be defined as the number of photobleached molecules divided by the number of absorbed photons.[47] The values of Φ_{ph} were determined by the absorption methodology (see ref 48 for details) based on the corresponding dynamic changes in the absorption spectra of **1** and **2** under irradiation and can be calculated as[48]

$$\Phi_{ph} = \frac{[D(\lambda, 0) - D(\lambda, t_0)]\cdot N_A}{10^3\cdot\varepsilon(\lambda)\cdot\int_\lambda\int_0^{t_0} I(\lambda)\cdot[1 - 10^{-D(\lambda,t)}]\cdot d\lambda\cdot dt} \quad (1)$$

where $D(\lambda,0)$ and $D(\lambda, t_0)$ are the values of sample absorbance at the excitation wavelength, λ, before and after the irradiation time period, t_0; $\varepsilon(\lambda)$, N_A, and $I(\lambda)$ are the extinction

https://doi.org/10.1021/acsomega.3c00654
ACS Omega 2023, 8, 11564−11573

Scheme 1. (i) (a) Br_2, EtOH, ∼45 °C; (b) $NCCH_2C(S)NH_2$, MgO, EtOH, Reflux; (ii) (a) 2,4-Dihydroxybenzaldehyde, Piperidine, MeOH, Reflux, (b) HCl, DMF, 70−75 °C, and (c) NaOH, H_2O−MeOH; and (iii) Me_2SO_4, K_2CO_3, DMF, 50−60 °C

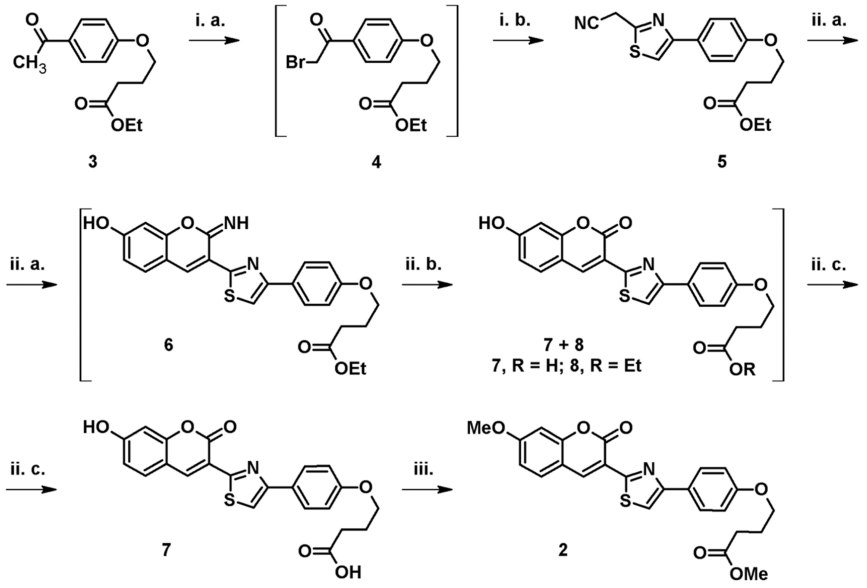

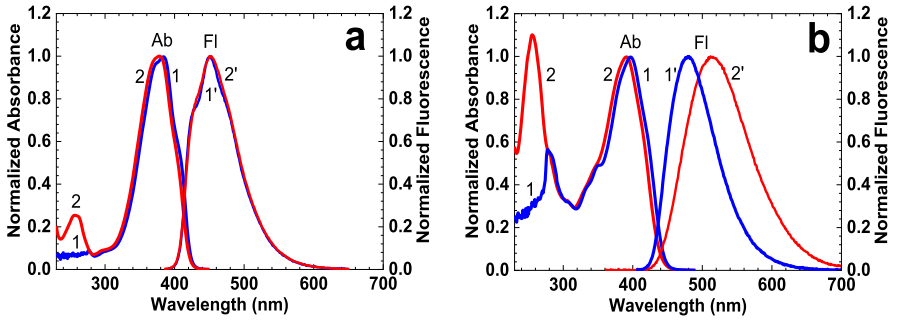

Figure 2. Normalized steady-state linear 1PA (1, 2) and corrected fluorescence (1′, 2′) spectra of coumarin derivatives **1** (a) and **2** (b) in BNZ (1, 1′) and ACN (2, 2′).

coefficient, Avogadro's number, and excitation irradiance per unit wavelength, respectively.

2.2. Spectroscopic Transient Absorption Pump−Probe and 2PA Measurements. The processes of ultrafast vibronic relaxations in the excited electronic states of **1** and **2** along with the corresponding time-resolved excited state absorption (ESA) spectra were investigated using the femtosecond transient absorption pump−probe technique, which was previously described.[49,50] In short, a femtosecond laser beam from a Ti/sapphire regenerative amplifier Legend F-1K-HE (Coherent, Inc.) with an output wavelength at ≈800 nm, pulse duration, $\tau_P \approx 140$ fs (fwhm), pulse energy, $E_P \approx 1.5$ mJ, and a 1 kHz repetition rate was split in two parts. The frequency of the first beam was doubled (1 mm BBO crystal) to produce an ≈400 nm pump beam ($E_P \approx 10$ μJ). The second beam was focused into a 2 mm sapphire plate to create a white-light continuum, which was used as a probe beam with $E_P \leq 5$ nJ. The pump and probe pulses were overlapped at a small angle in the sample cuvette (1 mm flow cell), and an optical delay line M-531.DD (PI, Ltd.) was used to create a variable time delay between these pulses. Transient absorption spectra were detected with a spectrometer (Acton SP2500i) and a CCD camera Spec-10 (Princeton Instruments, Inc.) The total temporal resolution of the employed experimental setup was estimated as ≤350 fs.

The degenerate 2PA spectra of **1** and **2** were measured in ACN at room temperature by an open aperture Z-scan method,[51] using 1 mm path length quartz cells with dye concentrations, $C \sim 10^{-2}$ to 10^{-3} M. These measurements were performed with the second harmonic (1 mm BBO crystal) of a 1 kHz laser beam from an optical parametric amplifier Opera-F (Coherent, Inc.) pumped by Coherent Legend F-1K-HE (output parameters: $E_P \leq 5$ μJ, $\tau_P \sim 100$−120 fs (fwhm) and tuning range 600−950 nm). The Z-scan setup was calibrated with a ZnTe standard.

2.3. Details of Quantum-Chemical Analysis of 1 and 2. The main electronic parameters of coumarin structures **1** and **2** were calculated based on the Gaussian 2009 suite of programs.[52] Quantum-chemical analysis of both molecules was performed for the corresponding model structures **1′** and **2′**, where the long non-conjugated substituents (linked with the main conjugated cyclic system by the $-CH_2$-linker) were simplified by the CH_3 group. DFT with the 6-31 G(d,p) basis set and the B3LYP functional was used for geometry optimization in the ground electronic state. TD-DFT was employed to describe the excited state (including geometry optimization). The entire set of linear spectral characteristics

https://doi.org/10.1021/acsomega.3c00654
ACS Omega 2023, 8, 11564−11573

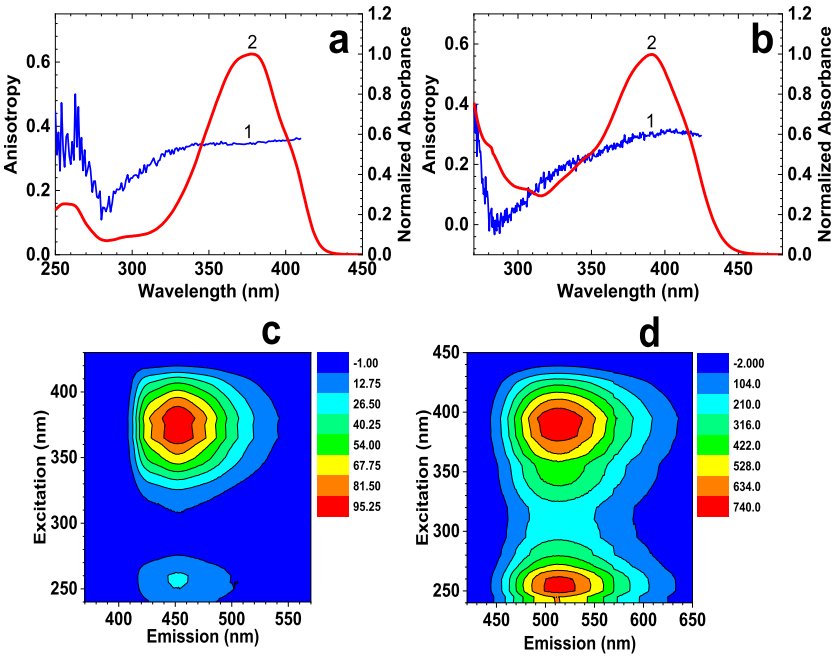

Figure 3. Steady-state excitation anisotropy (1) and 1PA (2) spectra of **1** (a) and **2** (b) in glycerol (1) and ACN (2). 3D fluorescence emission maps of **1** (c) and **2** (d) in ACN.

was predicted using optimized ground and first-excited singlet-state molecular geometry for absorption and emission spectra, respectively, along with the values of transition dipoles, oscillator strengths, orbital configurations, etc. All calculations were performed in vacuo and in acetonitrile. Solvent effects were taken into account with a polarizable continuum model in solvent model density parametrization.[53]

3. RESULTS AND DISCUSSION

3.1. Linear Spectroscopy and Photochemical Properties of 1 and 2. The main spectral parameters and the

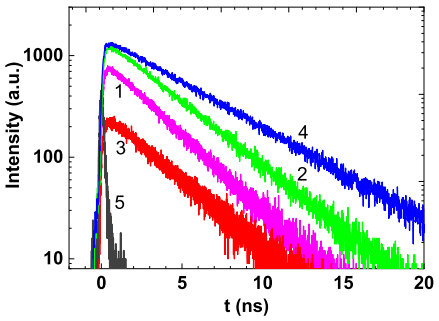

Figure 4. Fluorescence emission decays of coumarin derivatives **1** (1, 2) and **2** (3, 4) in BNZ (1, 3) and ACN (2, 4). Instrument response function (5).

corresponding values of photodecomposition quantum yields, Φ_{ph}, are shown in Figures 2–4 and Table 1. The steady-state linear one-photon absorption (1PA) spectra of **1** and **2** (Figure 2, curves 1, 2) revealed relatively weak long wavelength absorption bands at ~380–395 nm (maximum extinction coefficient, $\varepsilon^{max} \approx (24–28) \times 10^3$ M^{-1} cm^{-1}), with nearly structureless absorption contours and no substantial dependence on solvent polarity, which is typical for 3-thiazolylcoumarins in liquid medium at room temperature.[38,44,45] These 1PA bands can be attributed to a single $\pi \rightarrow \pi^*$ electronic

Table 1. Main Spectral and Photochemical Characteristics of Coumarin Derivatives 1 and 2 in BNZ and ACN: Absorption λ_{ab}^{max} and Fluorescence λ_{fl}^{max} Maxima, Values of Stokes Shifts, Maximum Extinction Coefficients ε^{max}, Fluorescence Quantum Yields Φ_{fl}, Transition Dipole Moments μ_{01}, Experimental τ_{fl}, and Calculated τ_{fl}^{cal}, Fluorescence Lifetimes, and Photodecomposition Quantum Yields Φ_{ph}

compound	1		2	
solvent	BNZ	ACN	BNZ	ACN
λ_{ab}^{max}, nm	385 ± 1	379 ± 1	395 ± 1	391 ± 1
λ_{fl}^{max}, nm	451 ± 1	450 ± 1	479 ± 1	515 ± 1
Stokes shift, nm (cm^{-1})	66 ± 2 (≈3800)	71 ± 2 (≈4160)	84 ± 2 (≈4440)	124 ± 2 (≈6160)
$\varepsilon^{max} \times 10^{-3}$, $M^{-1}\cdot cm^{-1}$	25.5 ± 2	27 ± 2	28 ± 2	24 ± 2
Φ_{fl}, %	63 ± 5	77 ± 5	45 ± 5	32 ± 5
μ_{01}, Debye	6.4	6.6	7.4	6.7
τ_{fl}, ns[a]	2.9 ± 0.1	3.5 ± 0.1	3.5 ± 0.1	4.9 ± 0.1
τ_{fl}^{cal}, ns	2.4 ± 0.5	3.3 ± 0.5	1.6 ± 0.5	2.0 ± 0.5
$\Phi ph \times 10^4$	1.7 ± 0.2	1.5 ± 0.2	0.6 ± 0.1	1.6 ± 0.2

[a]Excitation wavelength, $\lambda_{ex} \approx 400$ nm.

transition $S_0 \rightarrow S_1$ in accordance with nearly constant values of excitation anisotropy $r_0(\lambda)$ (see Figure 3a,b, curves 1) over the spectral range $\lambda \geq 330–350$ nm. These values of $r_0(\lambda) \approx 0.3–0.35$ are close to the theoretical limit[46] and related to the comparatively small angle between the absorption and emission transition dipoles for $S_0 \rightarrow S_1$ and $S_1 \rightarrow S_0$ electronic transitions, respectively. The intensity of the main long wavelength 1PA bands of **1** and **2** is connected to the absorption transition dipole, which can be estimated from the experimental data as:[54] $\mu_{01} \approx 0.096 \cdot \sqrt{\int \varepsilon(\nu) \cdot d\nu / \nu^{max}}$ (where the extinction coefficient $\varepsilon(\nu)$ is in M^{-1} cm^{-1}, ν is in cm^{-1}, and $\nu^{max} = 1/\lambda_{ab}^{max}$); the corresponding values are presented in Table 1. It should be mentioned that no aggregation effects

https://doi.org/10.1021/acsomega.3c00654
ACS Omega 2023, 8, 11564–11573

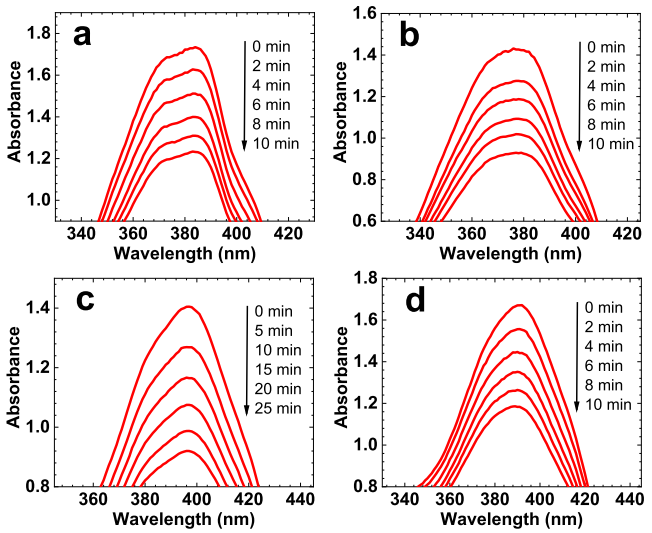

Figure 5. Consecutive changes in the 1PA spectra of **1** (a,b) and **2** (c,d) under CW laser irradiation in BNZ (a,c) and ACN (b,d) and corresponding irradiation times.

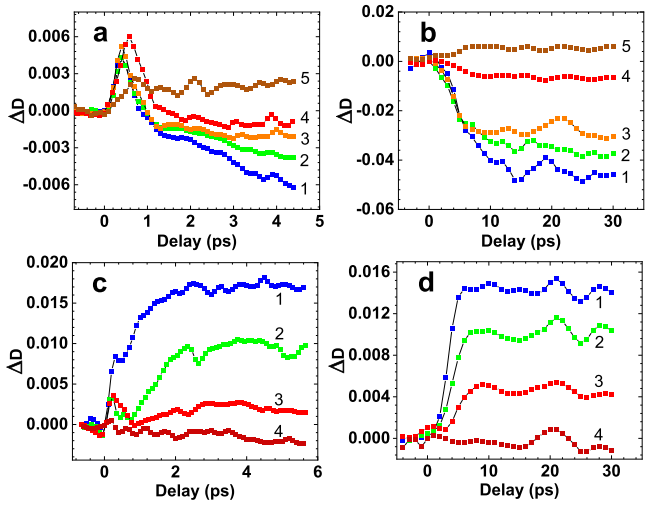

Figure 6. Transient absorption curves for **1** (a,b) and **2** (c,d) in ACN for specific probe wavelengths, λ_{pr}, at femtosecond (a,c) and picosecond (b,d) resolution: (a,b) λ_{pr} = 490 (1), 500 (2), 530 (3), 550 (4), and 580 nm (5); (c,d) λ_{pr} = 480 (1), 500 (2), 520 (3), and 550 nm (4).

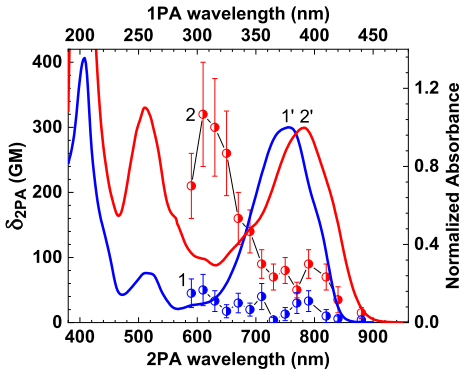

Figure 7. Degenerate 2PA spectra of **1** (1) and **2** (2) in ACN obtained by the femtosecond Z-scan method. Normalized steady-state 1PA spectra of **1** (1′) and **2** (2′) in ACN.

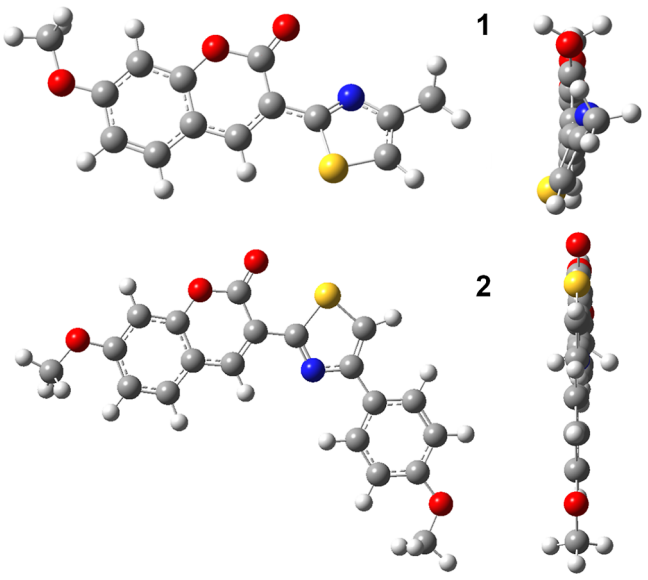

Figure 8. Optimized molecular geometries for the model structures of **1** (1) and **2** (2) in ACN (two projections) in the ground electronic state S_0.

were detected in the linear absorption spectra up to $C \sim 10^{-3}$ M.

The steady-state fluorescence spectra of **1** and **2** (Figure 2, curves 1′, 2′) exhibited a nearly structureless shape, relatively large Stokes shifts (~4000−6000 cm^{-1}), and were independent of the excitation wavelength in accordance with Kasha's rule.[46] 3D fluorescence maps of **1** and **2** (Figure 3c,d) also confirm this statement, along with the corresponding independence of the observed wavelength for the excitation spectra. It should be mentioned that coumarin derivative **1** revealed no solvatochromic behavior in contrast to derivative **2**, where a noticeable bathochromic shift was observed with an increase in solvent polarity. The observed spectral characteristics provide grounds for the substantial rearrangement of the optimized molecular geometry of **1** and **2** and a noticeable change in the value of permanent dipole moment for **2** under electronic excitation $S_0 \rightarrow S_1$. The values of the fluorescence quantum yields, Φ_{fl}, of **1** and **2** (Table 1) were independent of the excitation wavelength while exhibiting a complicated dependence on solvent polarity with a noticeable decrease in the polar solvent for **2**. The processes of spontaneous fluorescence emission were characterized by a single exponential profile (Figure 4) with the corresponding lifetimes, τ_{fl}, in the range ≈3−5 ns (Table 1). As deduced from these data, the values of τ_{fl} increase with solvent polarity, especially for **2** in ACN. It should be mentioned that τ_{fl} can be estimated theoretically based on linear molecular spectral data as:[46] $\tau_{fl}^{cal} = \tau_N \cdot \Phi_{fl}$, where τ_N is a natural lifetime, which can be calculated from the Strickler and Berg approach presented in ref 55. The obtained values of τ_{fl}^{cal} were sufficiently close to the corresponding experimental ones for **1** in both solvents and exhibit noticeable deviations for **2** (see Table 1), presumably due to a stronger rearrangement of the optimized molecular geometry in the excited electronic state S_1.[55,56]

The level of photostability for **1** and **2** was determined by the absorption method[48] using consecutive changes in the 1PA spectra under laser irradiation (Figure 5) and eq 1; calculated values of the photodecomposition quantum yields, Φ_{ph}, are summarized in Table 1. It is worth mentioning that the

https://doi.org/10.1021/acsomega.3c00654
ACS Omega 2023, 8, 11564−11573

Table 2. Calculated Values of the Electronic Parameters for Model Molecular Structures 1′ and 2′ in Vacuo and ACN: Transition Types and Wavelengths, λ, Oscillator Strengths, f, Transition Dipoles, μ, and the Main Orbital Configurations (HOMOs and LUMOs Stand for the Highest Occupied and the Lowest Unoccupied Molecular Orbitals, Correspondingly)

						components			
molec.	media	transition (type; A/F)[a]	λ, nm	F	$\lvert\mu\rvert$, D	μ_x	μ_y	μ_z	main configurations
1′	vacuo	$S_0 \rightarrow S_1$ ($\pi \rightarrow \pi^*$; A)	388	0.5558	6.769	6.759	−0.180	0.338	0.99|HOMO → LUMO⟩
		$S_0 \rightarrow S_2$ ($\pi \rightarrow \pi^*$; A)	322	0.0043	0.542	−0.539	0.058	−0.013	0.63|HOMO − 1 → LUMO⟩ +0.76|HOMO − 2 → LUMO⟩
		$S_0 \rightarrow S_3$ ($\pi \rightarrow \pi^*$; A)	312	0.0309	1.431	−1.430	−0.025	−0.056	0.72|HOMO − 1 → LUMO⟩ −0.58|HOMO − 2 → LUMO⟩
		$S_1 \rightarrow S_0$ ($\pi \rightarrow \pi^*$; F)	413	0.5401	6.884	6.877	−0.135	−0.269	0.99|HOMO → LUMO⟩
	ACN	$S_0 \rightarrow S_1$ ($\pi \rightarrow \pi^*$; A)	367	0.6965	7.369	7.351	−0.330	0.389	0.99|HOMO → LUMO⟩
		$S_0 \rightarrow S_2$ ($\pi \rightarrow \pi^*$; A)	304	0.0156	1.004	1.000	0.010	−0.084	0.94|HOMO − 1 → LUMO⟩
		$S_0 \rightarrow S_3$ ($\pi \rightarrow \pi^*$; A)	292	0.0425	1.624	−1.612	0.191	−0.048	0.82|HOMO − 2 → LUMO⟩
		$S_1 \rightarrow S_0$ ($\pi \rightarrow \pi^*$; F)	422	0.6457	7.609	7.599	−0.249	−0.302	0.99|HOMO → LUMO⟩
2′	vacuo	$S_0 \rightarrow S_1$ ($\pi \rightarrow \pi^*$; A)	441	0.2149	4.487	−4.175	1.643	0.003	0.99|HOMO → LUMO⟩
		$S_0 \rightarrow S_2$ ($\pi \rightarrow \pi^*$; A)	345	0.6061	6.665	−6.122	2.635	0.003	0.97|HOMO − 1 → LUMO⟩
		$S_0 \rightarrow S_3$ ($\pi \rightarrow \pi^*$; A)	302	0.0092	0.768	−0.535	0.551	0.000	0.70|HOMO − 3 → LUMO⟩
		$S_1 \rightarrow S_0$ ($\pi \rightarrow \pi^*$; F)	551	0.1641	4.383	−4.168	1.357	0.000	0.99|HOMO → LUMO⟩
	ACN	$S_0 \rightarrow S_1$ ($\pi \rightarrow \pi^*$; A)	432	0.3179	5.402	−4.922	2.227	0.003	0.99|HOMO → LUMO⟩
		$S_0 \rightarrow S_2$ ($\pi \rightarrow \pi^*$; A)	352	0.6254	6.839	−6.190	2.907	0.003	0.99|HOMO − 1 → LUMO⟩
		$S_0 \rightarrow S_3$ ($\pi \rightarrow \pi^*$; A)	307	0.0057	0.610	−0.013	0.610	0.000	0.97|HOMO − 3 →LUMO⟩
		$S_1 \rightarrow S_0$ ($\pi \rightarrow \pi^*$; F)	526	0.2135	4.884	−4.542	1.796	0.000	0.99|HOMO → LUMO⟩

[a]A—absorption/F—fluorescence.

observed photodecomposition processes corresponded to a first-order photoreaction,[57] and no substantial photoproducts were detected in the main absorption bands. According to these data, all values of Φ_{ph} are of the order of $\sim 10^{-4}$, comparable with the corresponding parameters of common laser dyes[58,59] and can be used in practice.

3.2. Fast Relaxations in the Excited States and 2PA Spectra of 1 and 2. The processes of fast vibronic relaxations in the molecular structures of **1** and **2** were investigated in ACN at room temperature using a well-developed pump−probe technique[49,50] and femtosecond excitation (temporal resolution ≤ 350 fs). Typical transient absorption dependences of the induced optical density, ΔD, on the temporal delay between pump and probe pulses, τ_D, are presented in Figure 6 for specific probe wavelengths, λ_{pr}. From these data, the kinetic changes in transient absorption curves revealed a fast temporal increase in ΔD (∼400−500 fs), which can be attributed to the dominant role of ESA processes with subsequent decreases (up to negative ΔD) for **1** (Figure 6a,b) or increases for **2** (Figure 6c,d) on the picosecond time scale over a broad spectral range (480−550 nm). Presumably, the observed positive ΔD signals in the first ∼0.5−1 ps are related to ESA processes from the unrelaxed Franck−Condon excited states.[60] The following 1−10 ps reflect simultaneous Franck−Condon[61] and solvate relaxation dynamics,[62,63] which result in nearly constant values of ΔD that slowly relax to zero in accordance with the corresponding lifetime of the S_1 state (i.e., on the nanosecond timescale). It is worth mentioning that negative ΔD signals for **1** (Figure 6b, curves 1−4) are evidence of possible light amplification (gain) processes, which can be potentially useful in superluminescence and lasing applications.[64,65] Nevertheless, no superluminescence phenomenon was observed for **1** in highly concentrated ACN solution under femtosecond excitation, likely due to a relatively weak radiative transition $S_1 \rightarrow S_0$ and the correspondingly high threshold for optical gain.[66] The time-resolved ESA spectra of **1** and **2** (Figure S11, see Supporting Information) exhibited no well-defined maxima at the specific wavelengths and were in good agreement between the spectral shape of optical gain, and the corresponding fluorescence contour was shown for **1**.

The degenerate 2PA spectra of **1** and **2** were obtained over a broad spectral range using an open aperture Z-scan technique[51] (Figure 7). The largest 2PA cross-sections, δ_{2PA}, for **1** (≈50 GM) and **2** (≈300 GM) were observed in the two-photon allowed short wavelength spectral range ∼590−650 nm, which corresponds to the lowest 1PA efficiency. It is worth noting that the molecular structures of **1** and **2** are not centrosymmetric, and noticeable values of $\delta_{2PA} \sim 50-100$ GM are observed in the one-photon-allowed main absorption bands. In general, 2PA efficiency can be estimated by the well-known sum-over-state approach,[67] according to which the value of δ_{2PA} in the main absorption band is roughly proportional to the product $\sim|\mu_{01}|^2|\Delta\mu_{01}|^2$ ($\Delta\mu_{01}$ is the change in the permanent dipole under electronic excitation $S_0 \rightarrow$

https://doi.org/10.1021/acsomega.3c00654
ACS Omega 2023, 8, 11564−11573

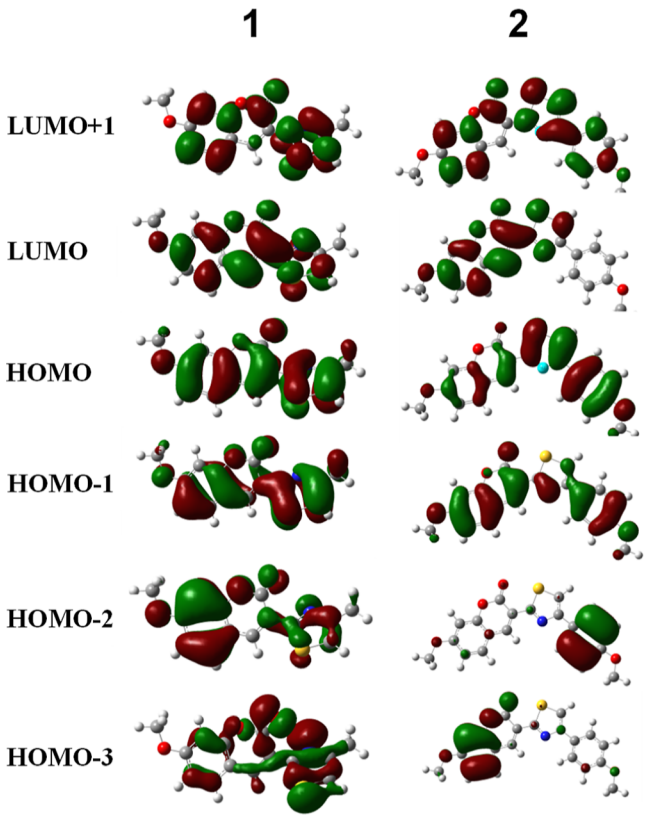

Figure 9. Calculated shapes of molecular orbitals for **1′** (**1**) and **2′** (**2**).

S_1).[68] Taking into account nearly identical values of μ_{01} for both coumarins (see Table 1), the larger values of δ_{2PA} for **2** in the main absorption band can be related to the larger $\Delta\mu_{01}$, which is consistent with its stronger solvatochromic behavior (see Figure 2). It should be mentioned that the obtained values of 2PA cross-sections are relatively large for **2** in the two-photon allowed spectral range and comparable with the corresponding parameters for 6,7-dimethoxy-substituted coumarin[42] and artificial coumarinic betalains.[43]

3.3. Theoretical Modeling of the Electronic Structures of 1 and 2. The electronic parameters of the model molecular structures **1′** and **2′** were estimated with the DFT/TD-DFT theoretical approach using optimized molecular geometries in the S_0 and S_1 electronic states for absorption and emission spectra, respectively. The shapes of the calculated optimized geometries of **1′** and **2′** in the ground electronic state (Figure 8) were sufficiently similar to the corresponding ones in the S_1 state except for the noticeable bond length changes (up to ∼0.06 Å) under electronic excitation, which can be responsible for the large Stokes shifts. According to the data in Figure 8, optimized structures of the model compounds exhibit almost planar molecular geometry, except for a small angle (≈26°) between the coumarin core and the thiazole substituent at the 3-position for **1′**. In both molecules, the first (long wavelength) electronic transition $S_0 \rightarrow S_1$ is of $\pi-\pi^*$ type, related to the pure electronic excitation (0.99|HOMO → LUMO⟩, see Table 2) and can be ascribed to the main absorption band. Significantly, there is no perfect match between the calculated and experimental spectral maxima, which is typical for the employed approach.[69,70] However, obtained values are sufficiently accurate to correctly analyze the nature of electron transitions in studied molecules. Following the data in Table 2, calculated transition dipoles μ_{01} (i.e., for excitation $S_0 \rightarrow S_1$) of **1′** and **2′** were sufficiently close to the corresponding ones estimated from the experimental spectral data (see Table 1), and no essential dependence of μ_{01} on solvent polarity was obtained. Based on the values of vector components μ_x, μ_y, and μ_z (see Table 2), the angles between absorption and emission transition dipoles can be determined for **1′** and **2′** in ACN as 3−6°, which is in good agreement with the excitation anisotropy spectral data (see Section 3.1). The change in the permanent dipole moment of **1′** under electronic excitation $S_0 \rightarrow S_1$ is relatively small (≈0.2 D) in contrast to the corresponding value of **2′** (≈1.2 D). This difference can be a reason for stronger solvatochromic behavior for **2** relative to **1**. The main molecular orbitals (MO) for **1′** and **2′** in Figure 9 reveal the nature of the first three electronic transitions. Following these data and the corresponding parameters in Table 2, in both model structures, the first excitation is practically a pure electron transition from HOMO to LUMO. The second and third transitions in **1′** are the combination of two electron configurations: HOMO − 1 → LUMO⟩ and HOMO − 2 → LUMO⟩, i.e., they correspond to transitions from two occupied MOs to the same vacant MO. All these MOs in **1′** are regularly delocalized along the total conjugated molecular structure, resulting in the largest oscillator strength for the $S_0 \rightarrow S_1$ transition and much weaker transitions $S_0 \rightarrow S_2$ and $S_0 \rightarrow S_3$ (Table 2). At the same time, in model structure **2′**, the LUMO is located primarily in the coumarin fragment, while all other highest occupied MOs are predominantly delocalized over the entire molecule, including the branch-conjugated substituent at position 3. These peculiarities lead to the largest intensity of the $S_0 \rightarrow S_2$ transition in comparison with $S_0 \rightarrow S_1$, which is in good agreement with experimental data. Importantly, the theoretical approach employed here quite reasonably described the majority of the major spectroscopic properties of coumarins **1** and **2**, providing validation for the computational methods.

4. CONCLUSIONS

The steady-state and time-resolved spectroscopic parameters and photochemical stability of 3-thiazolyl and 3-phenyltiazolyl coumarin derivatives **1** and **2** were comprehensively studied in solvents of different polarities at room temperature. Linear 1PA and fluorescence spectra, along with the 3D fluorescence maps, exhibited large Stokes shifts (up to 6000 cm^{-1}), and the nature of the chromophores' behavior can be considered "classical" (i.e., adherence to Kasha's rule). The steady-state excitation anisotropy spectra revealed only one electronic transition in the main long wavelength absorption band and nearly parallel orientations of the main absorption and emission transition dipoles. Fluorescence lifetimes, extinction coefficients, and the absorption and fluorescence spectra of hetarylcoumarin coumarin **1** were in good agreement with the Strickler and Berg relationships,[55] in contrast to coumarin **2**, where a relatively strong rearrangement of the molecular geometry in the excited electronic state can be assumed to predominate. The photostability of **1** and **2** in BNZ and ACN was in the range of $\Phi_{ph} \sim (0.6-1.7) \times 10^{-4}$, which is acceptable for practical applications.

Fast vibronic relaxation processes in **1** and **2** were finished in the first ∼5−10 ps and can be correlated to Franck−Condon and solvate reorganization dynamics. The potential of light amplification (gain) was observed for **1** without detection of

https://doi.org/10.1021/acsomega.3c00654
ACS Omega 2023, 8, 11564−11573

any superluminescence or lasing effects. The degenerate 2PA spectra of **1** and **2** were measured by an open aperture method, providing a maximum 2PA cross-section of ∼300 GM for **2**, which is quite suitable for two-photon-induced fluorescence microscopy imaging. Quantum-chemical DFT/TD-DFT analysis of coumarins **1** and **2** with heteroaromatic substituents confirmed the majority of the main experimental properties of the investigated compounds and can be proposed as a reasonable theoretical approach for the description of coumarin derivatives. Comprehensive investigations of the steady-state photophysical and photochemical properties, fast electronic relaxations in the excited states, the possibility of light amplification, and the reasonably high 2PA efficiency reveal the potential of these hetaryl coumarins for a number of photonic and biophotonic applications, including two-photon fluorescence bioimaging.

■ ASSOCIATED CONTENT

Supporting Information

The Supporting Information is available free of charge at https://pubs.acs.org/doi/10.1021/acsomega.3c00654.

Materials, instruments, and methods; NMR spectra; fluorescence decays, fits, and residuals; and time-resolved ESA spectra (PDF)

■ AUTHOR INFORMATION

Corresponding Authors

Kevin D. Belfield − *Department of Chemistry and Environmental Science, College of Science and Liberal Arts, New Jersey Institute of Technology, Newark, New Jersey 07102, United States;* orcid.org/0000-0002-7339-2813; Email: belfield@njit.edu

Mykhailo V. Bondar − *Institute of Physics National Academy of Sciences of Ukraine, Kyiv 03028, Ukraine;* orcid.org/0000-0001-6293-443X; Email: mbondar@mail.ucf.edu

Authors

Yevgeniy O. Shaydyuk − *Institute of Physics National Academy of Sciences of Ukraine, Kyiv 03028, Ukraine*

Nataliia V. Bashmakova − *Taras Shevchenko National University of Kyiv, Kyiv 01601, Ukraine*

George V. Klishevich − *Institute of Physics National Academy of Sciences of Ukraine, Kyiv 03028, Ukraine*

Andriy M. Dmytruk − *Institute of Physics National Academy of Sciences of Ukraine, Kyiv 03028, Ukraine*

Olexiy D. Kachkovsky − *V.P. Kukhar Institute of Bioorganic Chemistry and Petrochemistry of the NAS of Ukraine, Kyiv 02660, Ukraine*

Iaroslav B. Kuziv − *Institute of Molecular Biology and Genetics of the NAS of Ukraine, Kyiv 03141, Ukraine;* orcid.org/0000-0001-9381-1627

Igor Ya. Dubey − *Institute of Molecular Biology and Genetics of the NAS of Ukraine, Kyiv 03141, Ukraine*

Complete contact information is available at: https://pubs.acs.org/10.1021/acsomega.3c00654

Notes

The authors declare no competing financial interest.

■ ACKNOWLEDGMENTS

The authors thank the employees of the NASU Center for the collective use of equipment "Laser femtosecond complex" at the Institute of Physics, NAS of Ukraine, and Oleh Dmytruk for z-scan setup software development. This work is supported by the National Academy of Sciences of Ukraine (grants V/204). KDB acknowledges support from the US National Science Foundation (CHE-1726345), the National Institutes of Health (R21AA028340), and the Becton-Dickinson Research Professorship.

■ REFERENCES

(1) Pradhan, R.; Dahiya, H.; Bag, B. P.; Keshtov, M. L.; Singhal, R.; Sharma, G. D.; Mishra, A. Energy-Level Modulation of Coumarin-Based Molecular Donors for Efficient All Small Molecule Fullerene-Free Organic Solar Cells. *J. Mater. Chem. A* **2021**, *9*, 1563−1573.

(2) Liu, X.; Cole, J. M.; Low, K. S. Solvent Effects on the Uv−Vis Absorption and Emission of Optoelectronic Coumarins: A Comparison of Three Empirical Solvatochromic Models. *J. Phys. Chem. C* **2013**, *117*, 14731−14741.

(3) Sun, Y.-F.; Wang, H.-P.; Chen, Z.-Y.; Duan, W.-Z. Solid-State Fluorescence Emission and Second-Order Nonlinear Optical Properties of Coumarin-Based Fluorophores. *J. Fluoresc.* **2013**, *23*, 123−130.

(4) Kiraz, A. Ö.; Koca, M.; Kurt, A.; Kara, I.; Arıcı, C. Synthesis and Computational Studies on a Coumarin Derivative: 4-Chloromethyl Coumarin-7-Yl Methacrylate. *J. Mol. Struct.* **2022**, *1259*, 132702.

(5) Ibnaouf, K. H.; Prasad, S.; Aldwayyan, A. S.; AlSalhi, M. S.; Masilamani, V. Amplified Spontaneous Emission Spectra from the Superexciplex of Coumarin 138. *Spectrochim. Acta, Part A* **2012**, *97*, 1145−1151.

(6) Deshpande, A. V.; Jathar, L. V.; Rane, J. R. Effect of Matrix Treatment on Spectroscopic Properties of HCl Catalysed Sol-Gel Glasses Containing Coumarin Laser Dyes. *J. Fluoresc.* **2009**, *19*, 607−614.

(7) Hanczyc, P.; Słota, P.; Radzewicz, C.; Fita, P. Two-Photon Excited Lasing for Detection of Amyloids in Brain Tissue. *J. Photochem. Photobiol., B* **2022**, *228*, 112392.

(8) Abdallah, M.; Hijazi, A.; Graff, B.; Fouassier, J.-P.; Rodeghiero, G.; Gualandi, A.; Dumur, F.; Cozzi, P. G.; Lalevée, J. Coumarin Derivatives as Versatile Photoinitiators for 3D Printing, Polymerization in Water and Photocomposite Synthesis. *Polym. Chem.* **2019**, *10*, 872−884.

(9) Dumur, F. Recent Advances on Coumarin-Based Photoinitiators of Polymerization. *Eur. Polym. J.* **2022**, *163*, 110962.

(10) Gindre, D.; Iliopoulos, K.; Krupka, O.; Evrard, M.; Champigny, E.; Sallé, M. Coumarin-Containing Polymers for High Density Non-Linear Optical Data Storage. *Molecules* **2016**, *21*, 147.

(11) Hou, Y.; Wang, C.; Lu, J.; Jia, M.; Lv, Y.; Jia, X.; Zhu, Q.; Si, M.; He, H.; He, L. Design and Synthesis of First Environment-Sensitive Coumarin Fluorescent Agonists for MrgX2. *Int. J. Biol. Macromol.* **2022**, *203*, 481−491.

(12) Bourson, J.; Badaoui, F.; Valeur, B. Coumarinic Fluorescent Chemosensors for the Detection of Transition Metal Ions. *J. Fluoresc.* **1994**, *4*, 275−277.

(13) Kandemir, E.; Özkütük, M.; Aydıner, B.; Seferoglu, N.; Erer, H.; Seferoglu, Z. Novel Fluorescent Coumarin-Thiazole Based Sensors for Selective Determination of Cyanide in Aqueous Media. *J. Mol. Struct.* **2022**, *1249*, 131593.

(14) Srisuwan, P.; Sappasombut, A.; Thongyod, W.; Jantarat, T.; Tipmanee, V.; Leesakul, N.; Sooksawat, D. Highly Sensitive and Selective Coumarin-Based Fluorescent Chemosensor for Cu^{2+} Detection. *J. Photochem. Photobiol., A* **2022**, *427*, 113841.

(15) Ahmed, N.; Zareen, W.; Zhang, D.; Yang, X.; Ye, Y. Irreversible Coumarin Based Fluorescent Probe for Selective Detection of Cu^{2+} in Living Cells. *Spectrochim. Acta, Part A* **2022**, *264*, 120313.

(16) Manjunatha, B.; Bodke, Y. D.; Kumaraswamy, H. M.; Pasha, K. M. M.; Prashanth, N.; Kadam, P. R. Synthesis, Computational, Hepatoprotective, Antituberculosis and Molecular Docking Studies of Some Coumarin Derivatives. *J. Mol. Struct.* **2022**, *1254*, 132410.

(17) Eustáquio, R.; Ramalho, J. P. P.; Caldeira, A. T.; Pereira, A. New Red-Shifted 4-Styrylcoumarin Derivatives as Potential Fluorescent Labels for Biomolecules. *Molecules* **2022**, *27*, 1461.
(18) Pardo-Jiménez, V.; Navarrete-Encina, P.; Díaz-Araya, G. Synthesis and Biological Evaluation of Novel Thiazolyl-Coumarin Derivatives as Potent Histone Deacetylase Inhibitors with Antifibrotic Activity. *Molecules* **2019**, *24*, 739.
(19) Zou, Q.; Fang, Y.; Zhao, Y.; Zhao, H.; Wang, Y.; Gu, Y.; Wu, F. Synthesis and in Vitro Photocytotoxicity of Coumarin Derivatives for One- and Two-Photon Excited Photodynamic Therapy. *J. Med. Chem.* **2013**, *56*, 5288−5294.
(20) Fisher, W. G.; Partridge, W. P.; Dees, J. C.; Wachter, E. A. Simultaneous Two-Photon Activation of Type-I Photodynamic Therapy Agents. *Photochem. Photobiol.* **1997**, *66*, 141−155.
(21) Zhou, Z.; Tang, X.; Cui, Y.; Xue, S.; Yu, Z.; Li, Y. Blue Fluorescence from Pyridinyl Coumarincarboxymides Structure Having High Quantum Yield in Solution. *J. Mol. Struct.* **2022**, *1247*, 131229.
(22) Gawad, S. A. A.; Sakr, M. A. S. Spectroscopic Investigation, DFT and TD-DFT Calculations of 7-(Diethylamino) Coumarin (C466). *J. Mol. Struct.* **2022**, *1248*, 131413.
(23) Avdović, E. H.; Milanović, Z. B.; Molčanov, K.; Roca, S.; Vikić-Topić, D.; Mrkalić, E. M.; Jelić, R. M.; Marković, Z. S. Synthesis, Characterization and Investigating the Binding Mechanism of Novel Coumarin Derivatives with Human Serum Albumin: Spectroscopic and Computational Approach. *J. Mol. Struct.* **2022**, *1254*, 132366.
(24) Kitamura, N.; Fukagawa, T.; Kohtani, S.; Kitoh, S.-I.; Kunimoto, K.-K.; Nakagaki, R. Synthesis, Absorption, and Fluorescence Properties and Crystal Structures of 7-Aminocoumarin Derivatives. *J. Photochem. Photobiol., A* **2007**, *188*, 378−386.
(25) Liu, X.; Xu, Z.; Cole, J. M. Molecular Design of UV−vis Absorption and Emission Properties in Organic Fluorophores: Toward Larger Bathochromic Shifts, Enhanced Molar Extinction Coefficients, and Greater Stokes Shifts. *J. Phys. Chem. C* **2013**, *117*, 16584−16595.
(26) Offenbartl-Stiegert, D.; Clarke, T. M.; Bronstein, H.; Nguyen, H. P.; Howorka, S. Solvent-Dependent Photophysics of a Red-Shifted, Biocompatible Coumarin Photocage. *Org. Biomol. Chem.* **2019**, *17*, 6178−6183.
(27) González-Rodríguez, E.; Guzmán-Juárez, B.; Miranda-Olvera, M.; Carreón-Castro, M. D. P.; Maldonado-Domínguez, M.; Arcos-Ramos, R.; Farfán, N.; Santillan, R. Effect of the π-Bridge on the Light Absorption and Emission in Push-Pull Coumarins and on Their Supramolecular Organization. *Spectrochim. Acta, Part A* **2022**, *267*, 120520.
(28) Jhun, B. H.; Ohkubo, K.; Fukuzumi, S.; You, Y. Synthetic Control over Intra- and Intermolecular Charge Transfer Can Turn on the Fluorescence Emission of Non-Emissive Coumarin. *J. Mater. Chem. C* **2016**, *4*, 4556−4567.
(29) Ghosh, H. N.; Verma, S.; Nibbering, E. T. J. Ultrafast Forward and Backward Electron Transfer Dynamics of Coumarin 337 in Hydrogen-Bonded Anilines as Studied with Femtosecond UV-Pump/IR-Probe Spectroscopy. *J. Phys. Chem. A* **2011**, *115*, 664−670.
(30) Yamaji, M.; Hakoda, Y.; Okamoto, H.; Tani, F. Photochemical Synthesis and Photophysical Properties of Coumarins Bearing Extended Polyaromatic Rings Studied by Emission and Transient Absorption Measurements. *Photochem. Photobiol. Sci.* **2017**, *16*, 555−563.
(31) Krauter, C. M.; Möhring, J.; Buckup, T.; Pernpointner, M.; Motzkus, M. Ultrafast Branching in the Excited State of Coumarin and Umbelliferone. *Phys. Chem. Chem. Phys.* **2013**, *15*, 17846−17861.
(32) Oberhofer, K. E.; Musheghyan, M.; Wegscheider, S.; Wörle, M.; Iglev, E. D.; Nikolova, R. D.; Kienberger, R.; Pekov, P. S.; Iglev, H. Individual Control of Singlet Lifetime and Triplet Yield in Halogen-Substituted Coumarin Derivatives. *RSC Adv.* **2020**, *10*, 27096−27102.
(33) Han, J.; Cao, B.; Li, Y.; Zhou, Q.; Sun, C.; Li, B.; Yin, H.; Shi, Y. The Role Played by Solvent Polarity in Regulating the Competitive Mechanism between ESIPT and TICT of Coumarin (E-8-((4-Dimethylamino-Phenylimino)-Methyl)-7-Hydroxy-4-Methyl-2h-Chromen-2-one). *Spectrochim. Acta, Part A* **2020**, *231*, 118086.
(34) Harichandrana, G.; Surya, C. P.; Nehru, S. Synthesis, Photophysical Properties, Chemo-Sensing Ability and Computational Studies of Biscoumarin Derivatives. *J. Mol. Struct.* **2022**, *1248*, 131415.
(35) Ranjith, C.; Vijayan, K. K.; Praveen, V. K.; Kumar, N. S. S. Photophysical Investigation of 3-substituted 4-alkyl and/or 7-acetoxy Coumarin Derivatives-A Study of the Effect of Substituents on Fluorescence. *Spectrochim. Acta, Part A* **2010**, *75*, 1610−1616.
(36) Bahadur, A.; et al. Effect of Organic Solvents on Solvatochromic, Fluorescence, and Electrochemical Properties of Synthesized Thiazolylcoumarin Derivatives. *Luminescence* **2021**, *36*, 1189−1197.
(37) Mannekutla, J. R.; Mulimani, B. G.; Inamdar, S. R. Solvent Effect on Absorption and Fluorescence Spectra of Coumarin Laser Dyes: Evaluation of Ground and Excited State Dipole Moments. *Spectrochim. Acta, Part A* **2008**, *69*, 419−426.
(38) Doroshenko, A. O.; Posokhov, E. A.; Belokon', Y. V.; Kovalenko, S. N.; Ivanov, V. V.; Ponomarev, O. A. Ensembles of Rings with a Coumarin Unit. 2. Spectral Luminescent Properties and Spin-Orbit Coupling in Molecules of 3-(2-R-Thiazol-4-Yl)- and 3-(4-R-Thiazol-2-Yl) Coumarins. *Chem. Heterocycl. Compd.* **1997**, *33*, 1177−1184.
(39) Han, F.; Liu, W.; Zhu, L.; Wang, Y.; Fang, C. Initial Hydrogen-Bonding Dynamics of Photoexcited Coumarin in Solution with Femtosecond Stimulated Raman Spectroscopy. *J. Mater. Chem. C* **2016**, *4*, 2954−2963.
(40) Abdou, E. M.; Hafez, H. S.; Bakir, E.; Abdel-Mottaleb, M. S. A. Photostability of Low Cost Dye-Sensitized Solar Cells Based on Natural and Synthetic Dyes. *Spectrochim. Acta, Part A* **2013**, *115*, 202−207.
(41) Li, X.; Zhao, Y.; Wang, T.; Shi, M.; Wu, F. Coumarin Derivatives with Enhanced Two-Photon Absorption Cross-Sections. *Dyes Pigm.* **2007**, *74*, 108−112.
(42) Chitose, Y.; Abe, M.; Furukawa, K.; Katan, C. Design, Synthesis, and Reaction of π-Extended Coumarin-Based New Caged Compounds with Two-Photon Absorption Character in the near-IR Region. *Chem. Lett.* **2016**, *45*, 1186−1188.
(43) Rodrigues, A. C. B.; Mariz, I. F. A.; Maçoas, E. M. S.; Tonelli, R. R.; Martinho, J. M. G.; Quina, F. H.; Bastos, E. L. Bioinspired Water-Soluble Two-Photon Fluorophores. *Dyes Pigm.* **2018**, *150*, 105−111.
(44) Kuziv, I.; Dubey, L.; Dubey, I. Synthesis, Spectral Properties and Evaluation of Carboxy-Functionalized 3-Thiazolylcoumarins as Blue-Emitting Fluorescent Labeling Reagents. *Tetrahedron Lett.* **2020**, *61*, 152227.
(45) Kuziv, Y. B.; Ishchenko, V. V.; Khilya, V. P.; Dubei, I. Y. Synthesis of Reagents on the Basis of 7-Substituted 3-Thiazolylcoumarins for Covalent Labeling of Oligonucleotides. *Ukr. Bioorg. Acta* **2008**, *6*, 3−12.
(46) Lakowicz, J. R. *Principles of Fluorescence Spectroscopy*; Kluwer: New York, 1999.
(47) Chang, H.-J.; Bondar, M. V.; Liu, T.; Liu, X.; Singh, S.; Belfield, K. D.; Sheely, A.; Masunov, A. E.; Hagan, D. J.; Van Stryland, E. W. Electronic Nature of Neutral and Charged Two-Photon Absorbing Squaraines for Fluorescence Bioimaging Application. *ACS Omega* **2019**, *4*, 14669−14679.
(48) Corredor, C. C.; Belfield, K. D.; Bondar, M. V.; Przhonska, O. V.; Yao, S. One- and Two-Photon Photochemical Stability of Linear and Branched Fluorene Derivatives. *J. Photochem. Photobiol., A* **2006**, *184*, 105−112.
(49) Shaydyuk, Y. O.; Levchenko, S. M.; Kurhuzenkau, S. A.; Anderson, D.; Masunov, A. E.; Kachkovsky, O. D.; Slominsky, Y. L.; Bricks, J. L.; Belfield, K. D.; Bondar, M. V. Linear Photophysics, Two-Photon Absorption and Femtosecond Transient Absorption Spectroscopy of Styryl Dye Bases. *J. Lumin.* **2017**, *183*, 360−367.

https://doi.org/10.1021/acsomega.3c00654
ACS Omega 2023, 8, 11564−11573

(50) Bashmakova, N. V.; et al. Design and Electronic Structure of New Styryl Dye Bases: Steady-State and Time-Resolved Spectroscopic Studies. *J. Phys. Chem. A* **2014**, *118*, 4502−4509.
(51) Sheik-Bahae, M.; Said, A. A.; Wei, T. H.; Hagan, D. J.; Van Stryland, E. W. Sensitive Measurement of Optical Nonlinearities Using a Single Beam. *IEEE J. Quantum Electron.* **1990**, *26*, 760−769.
(52) Frisch, M. J.; et al. *Gaussian 09*, Revision A.2; Gaussian, Inc.: Wallingford CT, 2009.
(53) Marenich, A. V.; Cramer, C. J.; Truhlar, D. G. Universal Solvation Model Based on Solute Electron Density and on a Continuum Model of the Solvent Defined by the Bulk Dielectric Constant and Atomic Surface Tensions. *J. Phys. Chem. B* **2009**, *113*, 6378−6396.
(54) Hales, J. M.; Matichak, J.; Barlow, S.; Ohira, S.; Yesudas, K.; Brédas, J.-L.; Perry, J. W.; Marder, S. R. Design of Polymethine Dyes with Large Third-Order Optical Nonlinearities and Loss Figures of Merit. *Science* **2010**, *327*, 1485−1488.
(55) Strickler, S. J.; Berg, R. A. Relationship between Absorption Intensity and Fluorescence Lifetime of Molecules. *J. Chem. Phys.* **1962**, *37*, 814−822.
(56) Birks, J. B.; Dyson, D. J.; Flowers, B. H. The Relations between the Fluorescence and Absorption Properties of Organic Molecules. *Proc. R. Soc. London, Ser.* **1963**, *275*, 135−148.
(57) Ollis, D.; Mills, A.; Lawrie, K. Kinetics of Methylene Blue (MB) Photocatalyzed Reduction and Dark Regeneration in a Colorimetric Oxygen Sensor. *Appl. Catal., B* **2016**, *184*, 201−207.
(58) El-Daly, S. A.; El-Azim, S. A.; Elmekawey, F. M.; Elbaradei, B. Y.; Shama, S. A.; Asiri, A. M. Photophysical Parameters, Excitation Energy Transfer, and Photoreactivity of 1,4-Bis(5-Phenyl-2-Oxazolyl)-Benzene (POPOP) Laser Dye. *Int. J. Photoenergy* **2012**, *2012*, 458126.
(59) Azim, S. A.; Al-Hazmy, S. M.; Ebeid, E. M.; El-Daly, S. A. A New Coumarin Laser Dye 3-(Benzothiazol-2-Yl)-7-Hydroxycoumarin. *Opt. Laser Technol.* **2005**, *37*, 245−249.
(60) Vlček, A., Jr. The Life and Times of Excited States of Organometallic and Coordination Compounds. *Coord. Chem. Rev.* **2000**, *200−202*, 933−978.
(61) Wang, Y.; Liu, W.; Tang, L.; Oscar, B.; Han, F.; Fang, C. Early Time Excited-State Structural Evolution of Pyranine in Methanol Revealed by Femtosecond Stimulated Raman Spectroscopy. *J. Phys. Chem. A* **2013**, *117*, 6024−6042.
(62) Ghiasuddin; Akram, M.; Adeel, M.; Khalid, M.; Tahir, M. N.; Khan, M. U.; Asghar, M. A.; Ullah, M. A.; Iqbal, M. A Combined Experimental and Computational Study of 3-Bromo-5-(2,5-Difluorophenyl) Pyridine and 3,5-Bis(Naphthalen-1-Yl)Pyridine: Insight into the Synthesis, Spectroscopic, Single Crystal XRD, Electronic, Nonlinear Optical and Biological Properties. *J. Mol. Struct.* **2018**, *1160*, 129−141.
(63) Kumar, K. S.; Selvaraju, C.; Malar, E. J.; Natarajan, P. Existence of a New Emitting Singlet State of Proflavine: Femtosecond Dynamics of the Excited State Processes and Quantum Chemical Studies in Different Solvents. *J. Phys. Chem. A* **2012**, *116*, 37−45.
(64) Shaydyuk, Y. O.; Bashmakova, N. V.; Dmytruk, A. M.; Kachkovsky, O. D.; Koniev, S.; Strizhak, A. V.; Komarov, I. V.; Belfield, K. D.; Bondar, M. V.; Babii, O. Nature of Fast Relaxation Processes and Spectroscopy of a Membrane-Active Peptide Modified with Fluorescent Amino Acid Exhibiting Excited State Intramolecular Proton Transfer and Efficient Stimulated Emission. *ACS Omega* **2021**, *6*, 10119−10128.
(65) Kurhuzenkau, S. A.; Woodward, A. W.; Yao, S.; Belfield, K. D.; Shaydyuk, Y. O.; Sissa, C.; Bondar, M. V.; Painelli, A. Ultrafast Spectroscopy, Superluminescence and Theoretical Modeling of a Two-Photon Absorbing Fluorene Derivative. *Phys. Chem. Chem. Phys.* **2016**, *18*, 12839−12846.
(66) Shafer, F. P. *Dye Lasers*; Springer-Verlag: New York, 1973; p 285.
(67) Orr, B. J.; Ward, J. F. Perturbation Theory of Non-Linear Optical Polarization of an Isolated System. *Mol. Phys.* **1971**, *20*, 513−526.
(68) Ohta, K.; Antonov, L.; Yamada, S.; Kamada, K. Theoretical Study of the Two-Photon Absorption Properties of Several Asymmetrically Substituted Stilbenoid Molecules. *J. Chem. Phys.* **2007**, *127*, 084504.
(69) Fabian, J. TDDFT-Calculations of Vis/NIR Absorbing Compounds. *Dyes Pigm.* **2010**, *84*, 36−53.
(70) Jacquemin, D.; Zhao, Y.; Valero, R.; Adamo, C.; Ciofini, I.; Truhlar, D. G. Verdict: Time-Dependent Density Functional Theory "Not Guilty" of Large Errors for Cyanines. *J. Chem. Theory Comput.* **2012**, *8*, 1255−1259.

https://doi.org/10.1021/acsomega.3c00654
ACS Omega 2023, 8, 11564−11573